JOURNAL OF GEOPHYSICAL RESEARCH, VOL. 102, NO. B2, PAGES 2939–2951, FEBRUARY 10, 1997

Lithospheric structure of the Chaco and Paraná Basins of South America from surface-wave inversion

J. Arthur Snoke
Virginia Tech Seismological Observatory, Department of Geological Sciences
Virginia Tech, Blacksburg, Virginia

David E. James
Department of Terrestrial Magnetism, Carnegie Institution of Washington, Washington, D.C.

Abstract. Surface-wave data from a portable broadband array have been used to invert for the velocity structure of the crust and upper mantle beneath the Chaco and Paraná Basins of central South America. The upper-mantle velocity structure beneath the Paraná Basin is cratonic in character, whereas that beneath the Chaco Basin is tectonic or asthenospheric in character. The surface-wave analysis used broadband recordings from a subset of a 14-station array deployed in a roughly east-west sawtooth arrangement along 20°S latitude, with a total E-W aperture of ~1,400 km. Results from receiver-function analysis, as well as direct P-wave regional travel-time data, were used in the inversions to help constrain Moho depths and crust and upper-mantle velocities. S-wave structure for the intracratonic Paraná Basin was determined using interstation phase and group velocities for Rayleigh waves (fundamental and first higher mode) and Love waves (fundamental mode only) based on seven events with paths which traverse the eastern Paraná Basin and one event with a path across the western Paraná Basin. The average Moho depth in the eastern Paraná Basin is ~42 km. The high-velocity upper-mantle lid has a maximum S-wave velocity of 4.7 km/s, with no resolvable low-velocity zone to at least 200 km depth. This cratonic velocity structure indicates the presence of a lithospheric root beneath the Paraná Basin despite emplacement of the Paraná plume. The limited data from the western Paraná Basin are consistent with a homogeneous upper-mantle structure throughout the Paraná Basin. Waveform inversion of fundamental-mode and first-higher-mode Rayleigh waves from a single subandean event was used to obtain estimates for pure-path dispersion along propagation paths through the Chaco Basin and the western half of the Paraná Basin. The data were partitioned to isolate the partial-path contribution of the phase and group velocities for the Chaco Basin. The phase and group velocities from this somewhat sparse data set were inverted to obtain a velocity-depth model for the Chaco Basin. The distinguishing features of the Chaco model consist of a rather shallow Moho depth, 32 km, and low ("asthenospheric") upper-mantle S-wave velocities, about 4.2 km/s, with velocity increasing only slightly to about 4.3 km/s at 150 km depth.

Introduction

The tectonic development of the South American continent along the 20°S transect has been dominated by three major events: (1) the amalgamation of Gondwanaland (circa 600 Ma and subsequent); (2) the emplacement of the great Paraná plume and the opening of the South Atlantic (circa 135–125 Ma); and (3) the formation of the Andean orogen along the western margin of South America (circa 185 Ma–present). Present-day lithospheric structure is thus an integrated composite of the original deep continental structures modified by collision, plume emplacement, and the encroaching Andean orogen.

The surface-wave study presented here is based on data from an array of portable broadband seismic stations installed in south-central Brazil between 1992 and 1995 under the Brazilian Lithosphere Seismic Project (BLSP) to map heterogeneity of the lithosphere and upper mantle and correlate it with the principal tectonic provinces of the region (Figure 1). The entire region, including the Andean basement, comprises what is loosely termed the Brazilian shield, a patchwork of cratonic nu-

Paper number 96JB03180.
0148-0227/97/96JB-03180$09.00

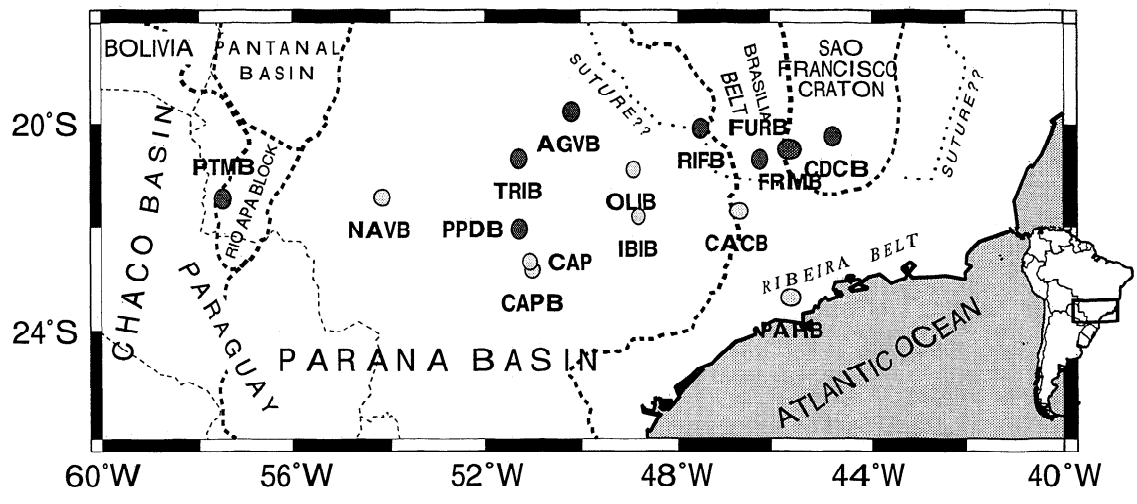

Figure 1. A schematic outline of the major geological provinces in southern Brazil. Locations of the Brazilian Lithosphere Seismic Project (BLSP) stations used in this study are shown as dark-gray circles; other BLSP stations are shown as light-gray circles. Recording systems consisted of dual-gain, 16-bit REFTEK data loggers with GPS timing and location. Sensors were all three-component broadband Streckeisen STS-2 seismometers. All stations except for NAVB were installed on bedrock.

clei of varying ages, most of which were amalgamated during late Proterozoic time (Brasiliano/Pan-African, circa 600 Ma), but some of which in the west and south were accreted through mid-Paleozoic time during the continuing consolidation of the Gondwana supercontinent [see *Brito Neves and Cordani*, 1991; *Ramos*, 1988]. The main geologic terranes west to east from the subandean zone include the low-lying Chaco Basin, a largely unstudied region blanketed by Phanerozoic sedimentary rocks; the poorly studied Rio Apa Block, a relatively small fragment of ancient crustal lithosphere that yields largely Proterozoic ages (circa 1.8–1.7 Ga) and is now exposed in a narrow belt between the Paraná and Chaco Basins; the intracratonic Paraná Basin; the Brasília Belt, a mobile belt of Proterozoic terranes mobilized during collision of the Paraná Basin and São Francisco craton in Brasiliano time (circa 600 Ma); and on the east, the São Francisco craton composed of Archean and Paleoproterozoic rocks. The two ancient continental blocks, the São Francisco craton and the Paraná Basin, appear to be contiguous at depth as evidenced by a steep Bouguer anomaly gradient interpreted by *Lesquer et al.* [1981] to be a cryptic collisional suture between the two units (shown as a dashed line labeled "Suture" in Figure 1). The intervening Brasília Belt is simply a collisional terrane. Prior to the BLSP series of studies, relatively little was known of lithospheric mantle structure across the region.

The purpose of the present work is to examine in detail the shear-wave velocity structure of the lithosphere beneath the Paraná and Chaco Basins. Although a previous tomographic study of SE Brazil based on the BLSP broadband data has shown that the São Francisco craton is underlain by a high-velocity root to at least 250 km [*VanDecar et al.*, 1995], in general, the velocity structure of the continental lithosphere to depths of about 200 km is not well resolved anywhere in the region. The lithospheric structure of the intracratonic Chaco and Paraná Basins is of particular interest because both provinces are something of an enigma. What, for example, is the nature of the crust and mantle beneath the low-lying Chaco Basin, what accounts for its lack of topographic relief, and what is its relationship to the encroaching Andean front? What is the deep structure of the Paraná Basin, and how was it affected by the Paraná plume? And to what depth is the lithosphere of these two provinces different? We are also concerned in this paper with determining the extent to which lateral heterogeneity can be observed in the lithosphere across the Paraná Basin.

The western part of the Chaco Basin is generally interpreted to be an Andean foreland basin developed mostly in Neogene time with a maximum subsidence of about 3 km at the Andean front. The subsiding foreland basin is about 100–120 km in width [*Coudert et al.*, 1995]. The sedimentary deposits in the western Chaco are clastic in nature and range from Oligocene to Recent in age [*Sempere et al.*, 1990; *Coudert et al.*, 1995]. The sub-Andean zone is actively overriding the western flank of the Chaco Basin, and the older deposits of the Chaco have now been partially incorporated into the sub-Andean fold and thrust belt. The undeformed preorogenic sedimentary section is "practically continuous from Silurian (the base of the section) to Mesozoic and Late Oligocene" [*Coudert et al.*, 1995, p. 280]. *Coudert et al.* [1995] estimate that the Andean "forebulge" has migrated at a rate of about 9–10 cm/yr for the past 9–10 Myr, or about 90 km into the western Chaco Basin. The underlying basement of the Chaco is part of the Pampean Terrane accreted to the Gondwana margin during Early Cambrian times [*Aceñolaza*, 1982; *Ramos*, 1988]. While the age of the collisional Pampean Terrane is moderately well constrained to about 500–600 Ma, the nature of the nucleus of the original

accreted block is poorly known. It appears likely, however, that the lithosphere of the Pampean Terrane may not have been as "cratonized" as that associated with the cratonic blocks to the east (Rio de la Plata, Paraná Basin, or São Francisco).

The Paraná Basin is wholly covered with Phanerozoic sedimentary rocks and Paraná flood basalts and therefore little is known of the geology of its 2+ Ga basement. Radiometric dating of rock samples from drill cores penetrating the basement led *Cordani et al.* [1984], *Brito Neves et al.* [1984], and their coworkers to infer a cratonic nucleus approximately in the axial region of the Paraná Basin, a region which includes stations PPBD, TRIB, and CAPB (Figure 1).

Of particular relevance to the present study is the work by *VanDecar et al.* [1995], based on travel time inversion of teleseismic body waves, that reveals a prominent vertical low velocity cylindrical structure in the upper mantle (200–500 km depth) beneath the NE Paraná Basin. VanDecar et al. interpreted the structure to be the "fossil" plume head conduit for the Paraná flood basalts [*VanDecar et al.*, 1995]. The location of the axis of the inferred conduit is near station OLIB shown in Figure 1. *Gallagher and Hawkesworth* [1992] and coworkers have suggested that the flood basalts were derived by plume melting of the hydrous lithospheric mantle beneath the Paraná Basin. If so, this melting event could have thermally eroded any preexisting high-velocity mantle root that may once have underlain the Paraná Basin. In general, *SKS* splitting measurements [*James and Assumpção*, 1996] show that present-day anisotropy of the Paraná Basin is very small. James and Assumpção interpreted the anisotropy to be comparatively young, possibly the result of outward flow from the axis of the plume head beneath the Paraná Basin. One objective of this study is to assess further on the basis of surface waves the possible extent of thermal erosion of the lithospheric keel during plume emplacement.

Data

The Brazilian Lithosphere Seismic Project utilized an array of stations deployed during the period November 1992 to June 1995 at 14 sites along a roughly east-west profile with an aperture of ~1400 km (Figure 1). A unique feature of the data set is the wealth of recordings of Andean earthquakes that illuminate the Brazilian shield. These Andean events are of particular value to the present study because the paths to the recording stations are wholly continental. Thus both body waves and surface waves, including higher modes, exhibit remarkably little attenuation, out-of-plane refraction, or multipathing so characteristic of waves with propagation paths traversing ocean-continent or other complex tectonic boundaries.

Three-component, broadband, 16-bit data were recorded continuously at 10 samples per second (sps) for all stations at high gain with a low-gain trigger to insure on-scale signals. Clipped high-gain records were patched with the low-gain data corrected for relative offset and magnification based on common non-clipped parts of the record. Horizontal components were then rotated into radial and transverse directions. The broadband STS-2 seismometers have flat velocity response from 0.008 to 50 Hz. All records were resampled, usually to 1 sps, using a zero-phase low-pass filter, and instrument corrected to displacement. The long-period response was stabilized with a zero-phase high-pass filter, with a corner typically at 0.005 Hz.

A summary of events used in this study is given in Table 1. Events were selected on the basis of both the quality of the data (absence of lengthy surface-wave codas so characteristic of multipathing and off-azimuth arrivals) and the requirement for interstation events that the great-circle propagation path for the event be no more than 3° off the great-circle path between the stations. In addition, we considered only interstation paths for which the station separation was at least 400 km, about one full wavelength at 100-s period. The station geometry and great-circle paths are shown in Figure 2. Table 2 provides a summary of azimuths and interstation distances and Table 3 provides a summary of Rayleigh and Love modes and period ranges for both group and phase velocities used in the analysis.

Data examples shown in Figure 3 are instrument-corrected and decimated vertical, radial, and transverse components for two events used in the study. Event 92333 is a comparatively nearby Andean event (see Figure 2), and 94043 is a very large teleseismic event. Note the near-perfect separation of Rayleigh and Love waves for both events. The good Rayleigh/Love separation is typical for Andean events but much less common for distant events, where the incidence angle across the coastline is critical. Event 94043 crossed the Chilean coast at near-normal incidence (see Figure 2), such that off-azimuth refractions were minimized.

Analytical Methods

In this work we employ two-station group- and phase-velocity inversion techniques as well as single-station,

Table 1. Hypocentral Information for Events Used in This Study

Event	Origin Time	Lat., °S	Long., °W	Depth, km	M_S
92333	0313:37.0	-31.395	-71.944	38.0	6.4
93049	1010:48.3	-0.472	-19.475	10.0	5.8
93074	1608:57.8	-26.790	-70.914	33.0	6.2
93275	0006:01.4	-24.038	-64.462	21.0	5.7
94036	2334:08.7	0.578	30.138	10.0	6.1
94043	0416:26.1	-10.777	-128.827	10.0	6.5
94241	1736:20.6	-0.439	-19.144	10.0	5.3
94344	0339:31.4	-23.579	-70.522	36.0	5.6

Individual event identifiers are made up of five-digit codes giving the year (first two numbers) and day of year (last three numbers) for the event. Origin times are in UT.

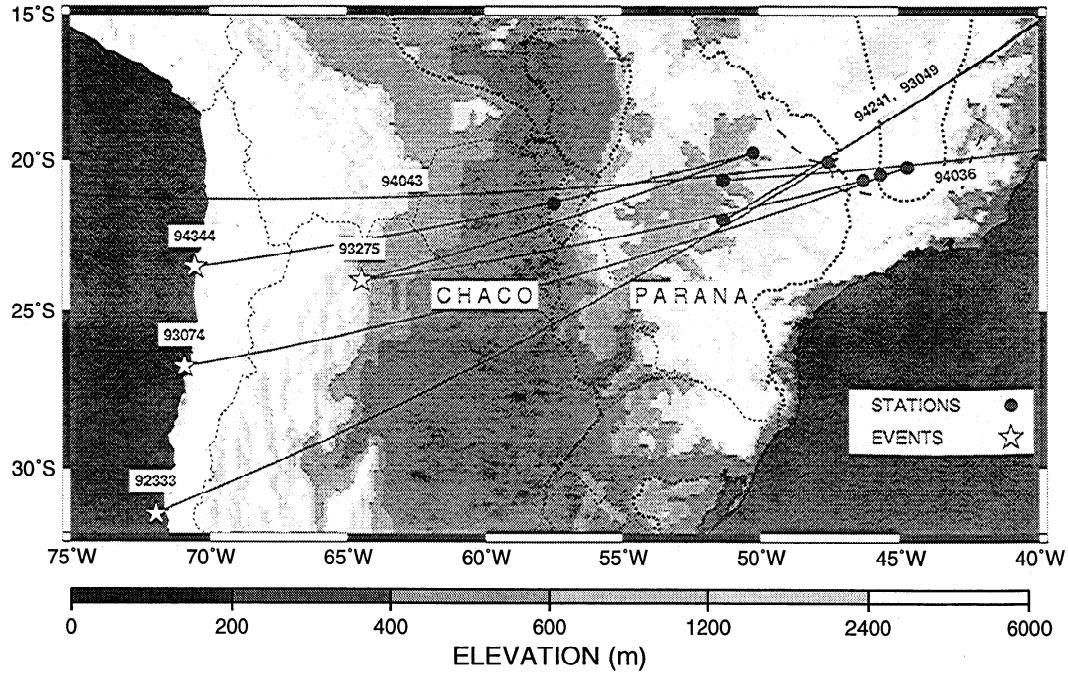

Figure 2. Pseudo-relief map showing the station locations, Andean event locations, and great-circle trajectories for surface-wave paths used in this study. Event names are keyed to Table 1. Upper-mantle S-wave velocity structure was determined in this study for both the Chaco and Paraná Basins.

multiple-mode waveform inversion. The interstation methods were used to solve for the S-wave velocity structure beneath the Paraná Basin. Results from these analyses were used in conjunction with waveform inversion from a well-recorded subandean event to determine the velocity structure beneath the Chaco Basin.

The two-station technique involves two stages: determination of interstation phase and group velocities and the inversion of these dispersion velocities to obtain the S-wave velocity-depth structure. Single-station group velocities were determined for the vertical (Rayleigh) and transverse (Love) components using frequency-time analysis (FTAN). The procedure follows that introduced by *Dziewonski et al.* [1969], enhanced by using instantaneous frequency (to allow for amplitude variations with frequency) and the display-enhancing filter introduced by *Nyman and Landisman* [1977] (whereby the Gaussian filter width is proportional to the square root of the period).

Table 2. Paraná Events

Event YYDDD	Station Name	Δ, km	Bk Az deg	δΔ, km
92333	PPDB	2262	239	451
	RIFB	2712	238	
93049	RIFB	3744	58	451
	PPDB	4196	60	
93074	PPDB	2054	251	712
	CDCB	2766	250	
93275	PPDB	1365	258	543
	FURB	1908	255	
94036	FRMB	8558	84	593
	TRIB	9150	86	
94043	TRIB	8310	264	404
	RIFB	8714	263	
94241	RIFB	3776	58	452
	PPDB	4227	60	
94344	PTMB	1362	258	779

Δ, epicentral distance; Bk Az, station-epicenter azimuth; and δΔ, interstation epicentral distance.

Figure 4 shows vertical-component FTAN displays for events 92333 and 94043. For 92333, group velocities are well constrained over a period range of 10–130 s for the Rayleigh fundamental mode, and for 94043 the usable range in group velocities is 40–200 s. For both cases the input-period display spacing is uniform in the log of the period. For event 94043 the amplitude decreases rapidly approaching periods around 200 s, so the instantaneous period correction shifts the "effective" period to lower values leading to closer spacing in the output periods. For example, the highest input period of 300 s was shifted to 200 s.

Appropriate time windows (or, equivalently, group-velocity windows) and period range were chosen on the basis of visual examination of the group velocity displays. The records were then filtered in both the time and period domains using full weight in the pass-band of interest and cosine tapers to minimize ringing. Preliminary estimates of interstation phase velocity were obtained by examining peak-trough correlations for Rayleigh or Love waves for the two stations on narrow band-pass filtered records at selected periods spanning the full period range of interest. This procedure is important both for quality control of the seismic

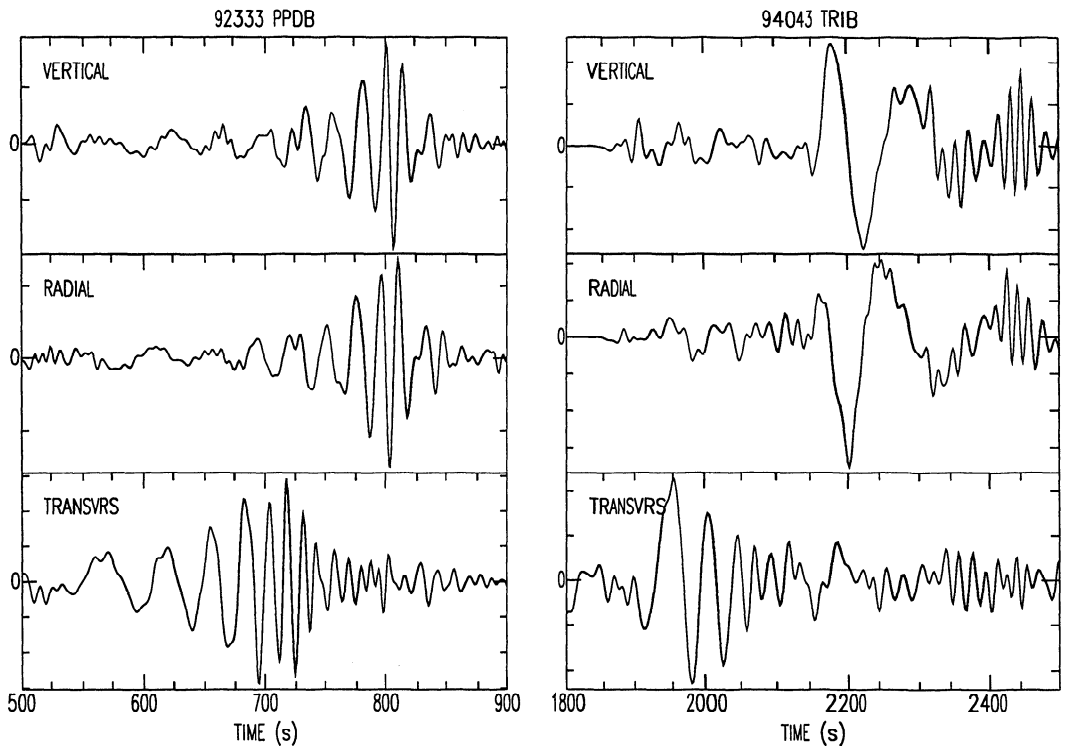

Figure 3. Vertical, radial, and transverse components for (left) event 92333 recorded at station PPDB and (right) event 94043 recorded at TRIB. Time traces have been decimated and instrument corrected to displacement. Note the near-perfect separation of Rayleigh and Love waves on the horizontal components and for event 92333 the absence of energy in the coda of the large-amplitude (minimum-group-velocity) Airy phase.

signal and also to insure that the calculated interstation phase velocities lie on the correct branch (i.e., no cycle skipping has occurred).

For each mode and station pair the processed waveformsare analyzed to obtain estimates of phase velocity and phase-velocity errors as a function of period based on smoothed autocorrelation and cross-correlation spectra [*Herrmann*, 1987]. A smoothing running average of three points sufficed in most instances. Where the phase velocity versus period curves had obvious "kinks", smoothing using up to seven or nine points was used.

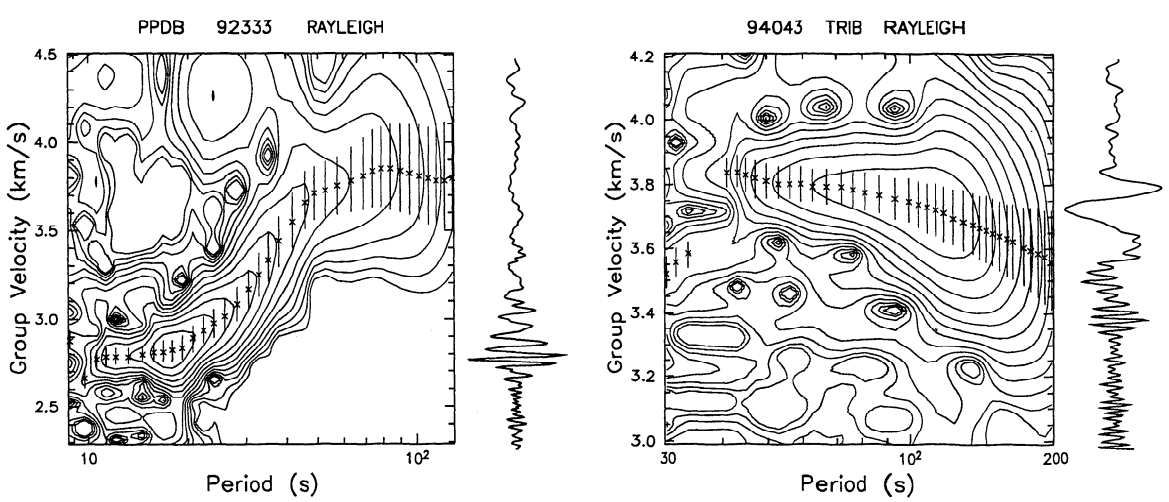

Figure 4. Frequency-time analysis (FTAN) for the instrument-corrected, vertical-component seismograms from the two events for which time series traces are shown in Figure 3. The x's are computer-picked energy maxima for each period, and the vertical lines are ±1 dB. Contours are spaced every 3 dB. The period range is 9–130 s for event 92333 and 30–200 s for event 94043. The vertical axis is group velocity.

It is desirable to use interstation group velocities in addition to phase velocities when inverting for structure because of the differences in the sensitivity to structure of the two velocities [e.g., *Bloch et al.*, 1969]. While interstation group velocities can be calculated from derivatives with respect to frequency of the phase velocities, the procedure tends to produce group velocities that are biased by fine structure in the phase velocity curves. We prefer instead a more stable method, less directly influenced by the phase velocities, whereby we calculate the interstation Green's functions [*Russell*, 1987; *Herrmann*, 1987; *Taylor and Toksoz*, 1982] and use FTAN on those functions to obtain a direct estimate of the interstation group velocity.

Interstation phase and group velocities are inverted to obtain average S-wave velocity-depth structure along the interstation profile [*Russell*, 1987; *Herrmann*, 1987] The inversion technique requires a starting velocity model with constant velocities in each layer. Throughout the inversion, the thickness and Poisson's ratios for each layer remained unchanged. The P-wave velocity is derived from the S-wave velocity and the Poisson's ratio, and the density is derived from the P-wave velocity. A continental-shield Q_S structure is assumed. All models assume spherical-Earth rather than flat-Earth geometry.

For single-station velocity inversions, group-velocity curves based on frequency-time analysis typically contain systematic errors (group delays) resulting from source duration and complexity, focal mechanism, and the like. (Such errors cancel out for the two-station techniques described above.) Moreover, body-wave interference and mixing of higher modes can adverseley affect the interpretation of group-velocity inversion. Accordingly, for single-station velocity inversion we use *Nolet*'s [1990] method of waveform inversion.

Results

The results summarized below are presented by region: (1) the eastern Paraná Basin, which encompasses the region of the basin east of the "axial" stations PPDB, TRIB, and AGVB; (2) the western Paraná Basin, extending westward from the axial stations to station PTMB; and (3) the Chaco Basin.

Eastern Paraná Basin

Seven events provide interstation phase and group velocities for the eastern Paraná Basin as summarized in Table 2. The range of usable periods is based on an examination of the error estimates and the shapes of the dispersion curves. Computed interstation group velocities were generally less stable then phase velocities and were well constrained over a smaller range of periods. The period ranges for the interstation phase and group velocities used in the inversion for velocity-depth structure are given in Table 3.

Interstation dispersion curves for individual events were fit using cubic-spline interpolation, and dispersion velocities were then determined at a common set of periods, with a spacing which increased with period as approximately the square root of the period. After interpolation to the standard set of periods, all values were used in the inversion, with no explicit weighting. The composite data set (Figure 5) had 70/48 fundamental-mode Rayleigh phase/group velocity values, four first higher-mode Rayleigh phase velocity values, and 38/21 fundamental mode Love phase/group velocity values.

Table 3. Period Ranges Used for Interstation Phase and Group Velocities for the Paraná Basin Paths Given in Table 2

Event	Mode	P_{1p}	P_{2p}	P_{1g}	P_{2g}
92333	R0	12	81	13	81
	L0	14	65	13	44
93049	R0	65	24	37	
93074	R0	12	137	13	81
	L0	14	81	24	44
93275	R0	21	91	21	53
	R1	7	13		
	L0	23	53	27	53
94036	R0	34	142	32	44
94043	R0	81	186		
	L0	34	103		
94241	R0	20	53	21	44
94344	R0	20	65		
	L0	10	43		

P_{1g}, minimum period used for interstation group velocity; P_{2p}, maximum period used for interstation phase velocity. All velocities are in kilometers per second. R0, fundamental-mode Rayleigh; R1, first higher-mode Rayleigh; L0, fundamental-mode Love.

The inversion routine requires a starting velocity model with constant-velocity layers. Crustal thickness for the starting model was based on receiver-function determinations at Brazilian stations [*James et al.*, 1993]. In general, receiver function results showed crustal thickness decreasing from about 45 km along the axis of the basin to about 40 km near the margins. Similarly, the thickness of the sedimentary rocks thinned from a maximum of about 5 km along the axis of the basin to zero at the margin of the basin. Mean crustal velocities appear to be similar over the region of the basin. On the basis of these results the starting model that included a 2-km low-velocity (sedimentary) layer at the surface, a two-layer crust with a midcrustal discontinuity at 20 km depth, and a Moho depth of 42 km. The Moho depth is not only averaged from receiver function results but appears to be a reliable estimate based on comparisons of errors and output velocity-model smoothness near the Moho for inversion runs assuming different Moho depths. The upper mantle in this region was not well constrained, so the starting model set V_S to 4.5 km/s for the upper mantle. In all modeling the Poisson's ratio was constrained to 0.25 in the crust and 0.27 in the mantle. Reasonable variation in Poisson's ratio did not alter results significantly.

For the initial model runs we used the differential smoothing option [see *Hwang and Mitchell*, 1987, pp.

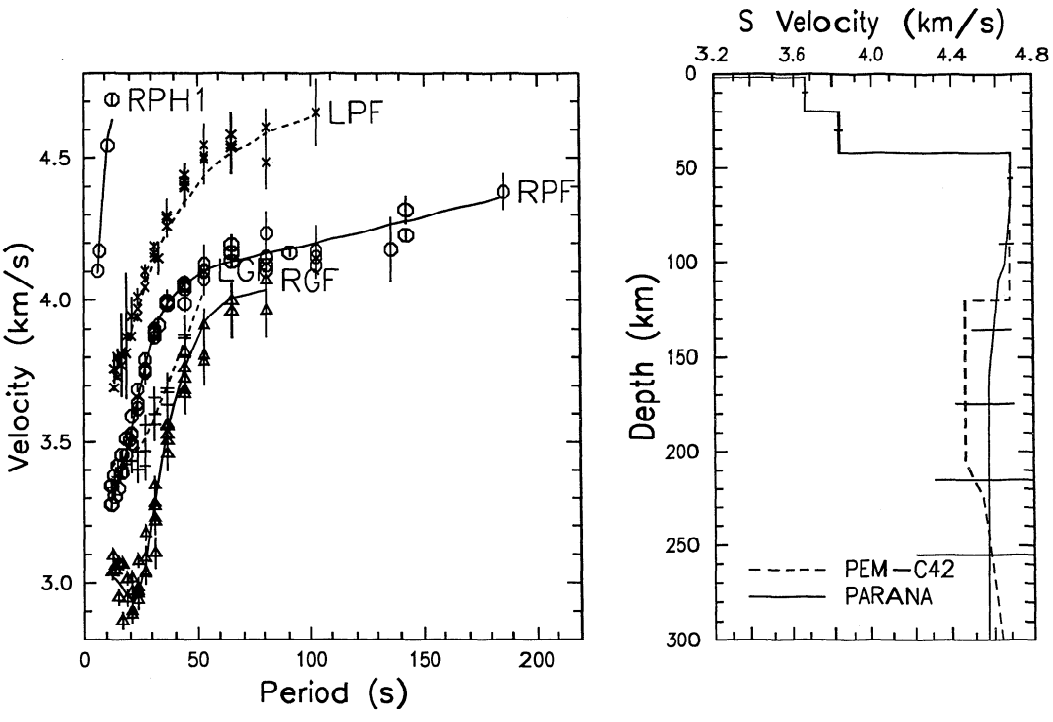

Figure 5. (left) Eastern Paraná interstation phase and group velocities versus period for the seven events used in the inversion for *S*-wave velocity. Fundamental Rayleigh-wave velocities were used for all seven events, first-higher-mode Rayleigh phase velocity for one event, and fundamental Love-wave velocities for four events. Line curves are calculated from the velocity model after inversion and are labeled according to R, Rayleigh; L, Love; P, Phase; G, Group; F, Fundamental; H, Higher-mode. (right) The final velocity-depth model with error estimates. Model PEM-C42 is included for reference. The displayed model layer transitions have been smoothed except for intended first-order discontinuities.

590–591]. As implemented in the nonlinear inversion code, velocity variations between adjacent layers are minimized such that the inversion will not produce large velocity steps between layers, but it will preserve starting-model discontinuities. This kind of smoothing couples the model parameters in a way that makes it difficult to interpret estimated errors and resolution. Hence in the final computations we used the no-smoothing, stochastic inversion option.

The starting model consisted of 50 layers over a uniform half-space starting at 400 km depth. No layers were more than 20 km thick. The large number of layers is advantageous in that it produces smoother models and also obviates the problem noted by *Mitchell* [1984] that coarse layering may make it difficult to invert Love and Rayleigh data simultaneously because of differences in the depth dependence of the dispersion partial derivatives with respect to velocity.

Estimates of Variance and Resolution for the Eastern Paraná Model

The 50 layers are the model parameters and the dispersion values are the data parameters. Error analysis for a least squares inversion assumes independence among both the model parameters and the data parameters. Neither condition is met here, but we feel plausible estimates of both the variance and resolution can be gotten from this analysis.

As noted above, for each event a cubic-spline fit is found for the dispersion velocities. The inversion requires discrete values for the dispersion data parameters, so dispersion at only a selected set of periods can be used. The chosen spacing in period, which increased as approximately the square root of the period, is such that the overlap of the gaussians used in the frequency-time group-velocity analysis on the observed waveforms is constant. With this choice the dependence among the "data parameters" is approximately uniform.

We assume that an estimate of the data variance is given by the variance of the (observed - calculated) dispersion values, for which the number of degrees of freedom are the number of model parameters. To calculate error estimates, the number of layers for the "final" model was reduced to eight, with layers organized to extend over given depth ranges for which the velocity variation was comparatively small. The final stochastic inversion involved a single iteration with program SURF's least squares damping coefficient set at 1.0. The residual errors in dispersion velocities were approximately the same as they were for the final run from the 50-layer model, and the predicted dispersion values were not significantly different. The standard deviations plotted in Figure 5 are based on the predicted next iteration with zero damping. Below 300 km depth the standard deviation estimated by this method is 0.5 km/s (in other words, we have no reliable estimate of the velocities at

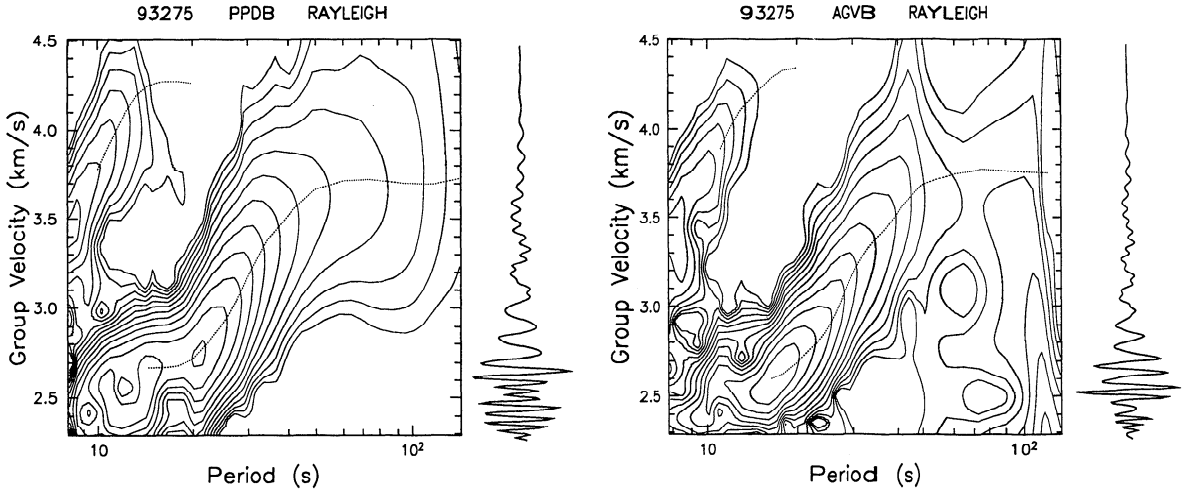

Figure 6. Frequency-time analysis, as in Figure 4, for the instrument-corrected, vertical-component seismograms from (left) PPDB and (right) AGVB for event 93275. The higher modes are visible on the time traces and well defined on the group-velocity plots. Lines show predicted group-velocities for the final models for each path over the frequency bandpasses applied to R0 and R1.

or beyond that depth). With zero damping one gets no formal estimate of the model resolution. From examination of the partial derivative of the phase and group velocities with S-wave velocity based on the 50-layer model we estimate that the overall resolution is approximately equal to the layer thicknesses in our final model, about 60 km in the uppermost mantle and over 100 km at depths below 150 km.

Western Paraná and Chaco Basins

Results for the western Paraná and Chaco Basins are derived from a single large shallow-focus sub-Andean event (93275, see Table 1) that was well recorded at several stations across the BLSP array (and was used above in the eastern Paraná inversion). Of particular interest here are the recordings at stations PPDB and AGVB, which are near the axis of the Paraná Basin (Figure 2). The propagation paths for the sub-Andean event to those stations cover the western Paraná and the whole of the Chaco Basin, two markedly different geologic provinces, necessitating structural partitioning of the paths.

Group-velocity displays for event 93275 recorded at PPDB and AGVB are shown in Figure 6. Results from the group velocity analysis constrain the period range for waveform inversion. At PPDB the group velocities are well constrained to periods beyond 100 s, and they become unreliable below 15 s. For AGVB there is less coherence at longer periods but slightly better behavior at shorter periods. For both stations the first higher Rayleigh mode is clear in both the time trace and the group velocity display over a period range from about 6 to 14 s.

The starting model for the waveform inversion included a low-velocity (sedimentary) layer 3.5 km thick, a midcrustal discontinuity at 20 km, and a Moho discontinuity at 37 km depth. The P-wave mantle velocities were fixed, based on a body-wave travel-time study for this region [*James*, 1994a, b]. The S-wave velocities for the starting model came from an inversion of the single-station group velocity. The constant-velocity layers are thin, none more than 10 km thick, to a depth of 415 km.

To use each layer as a model parameter would produce a very ill-conditioned matrix to be inverted. We accordingly follow *Nolet* [1981, 1990] and use instead a small set of model parameters which are overlapping, weighted averages over the velocity-depth model. These basis functions as used here are shown in Figure 7. The crust is covered by two parameters with uniform weighting over depth ranges 0–20 km and 20–37 km. The inversion is essentially insensitive to velocity contrasts at depths greater than 300 km, thus the uniform-weighted parameter over the depth range 300–415 km. Between 37 and 300 km we use five parameters with weighting as shown in Figure 7. Nolet's inversion scheme also allows one to include Moho depth as a variable. In preliminary runs a Moho-depth parameter was included, but depth changes were generally less than a kilometer. As statistical interpretation of the uncertainties and resolution is considerably simpler when the depth parameter is not included, it was not included in the final inversions.

Time windows were selected based on results of the group velocity determinations shown in Figure 6. The filtering procedure used in this study gives full weight to values within the frequency and time ranges of interest, with cosine tapering outside that range to minimize ringing. Although the waveform inversion is for a single event-station pair, up to four time-series traces can be used. Thus a single inversion can include not only Love and Rayleigh waves but also, for example, single-component traces that have been windowed and filtered to isolate higher modes and/or to isolate the relatively low-amplitude high periods for the fundamental mode. We modified the inversion code to allow different relative weights among the time-series traces.

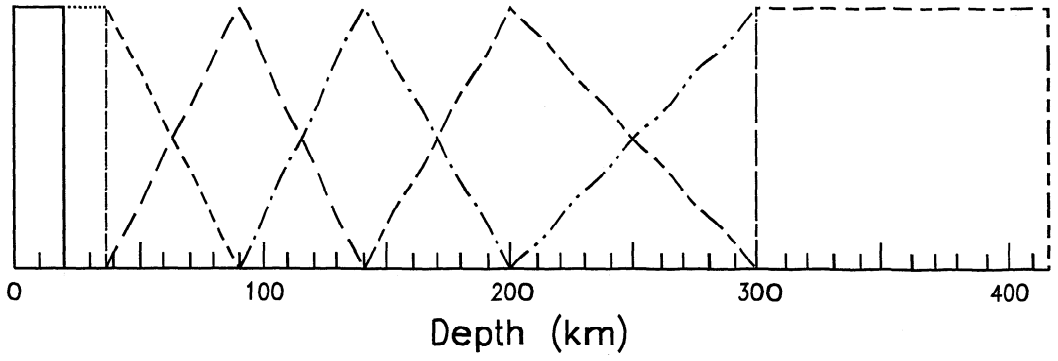

Figure 7. Interpolation model parameters (termed basis functions by *Nolet* [1990]) used in the waveform inversion. Of the eight parameters, three are "box car" in shape, resulting in uniform weighting throughout the depth range. Two of these are in the crust, and the third is over the depth range 300–415 km, which is below the depth range resolved by these data. The upper mantle, from 37 to 300 km, is spanned by five overlapping triangles, as shown.

The inversion is carried out by fixing the low end of the frequency band for each trace and iterating the inversion for increasing values of the high-cut frequency. The purpose of this procedure is to diminish the possibility of cycle skipping when matching data and synthetics. The final high-cut frequency selected is based on the statistics of the data/synthetics mismatch after each iteration. The goodness of fit between data and synthetics is evaluated by a weighted least squares difference of the time-domain traces. The weighting is effectively inversely proportional to the trace amplitude, thus giving greater weight to zero crossings than to peaks. All traces are normalized to the same total energy, so the waveform inversion provides no information about the actual size of the event.

Source depth and focal mechanism are required for the inversion. For event 92375 the focal depth (21 km) is from the PDE hypocenter, and the focal mechanism is from the Harvard CMT solution. That focal mechanism, given in terms of strike, dip, and rake, is 237°, 56°, and 179°. As can be seen in Figure 6, event 93275 generated large higher modes, so we generated a higher-mode seismogram, filtered in time and frequency, to be included in the analysis. We weighted the higher-mode traces at half the weight of the fundamental-mode traces.

Although event 93275 produced large Love-wave signals, initial results from the combined inversion of Rayleigh and Love waves yielded relatively poorer fits than those using only Rayleigh fundamental and first higher mode. The Love waves require higher velocities and/or a shallower Moho than do the Rayleigh waves. The cause of this may be anisotropy and/or the different sensitivies of Love and Rayleigh waves to the lateral heterogeneity which we show below exists along the paths. *SKS* splitting measurements [*James and Assumpção*, 1996] indicated varying degrees of azimuthal anisotropy (i.e., anisotropy in the horizontal plane) beneath the region, but nowhere was it very large. Surface-wave inversion programs that incorporate anisotropy, on the other hand, consider models in which only transverse (i.e., horizontal) isotropy and a vertical axis of symmetry are assumed, the only form of anisotropy which preserves a clean separation of Love and Rayleigh waves. Hence we cannot model the observed anisotropy, and the code we used can handle only isotropic structures. Experience from two-station analysis suggests, however, that the Rayleigh wave contribution to the solution is by far the dominant one, especially when a Rayleigh higher mode is included in the analysis.

Table 4 shows the group-velocity and frequency windows for the four Rayleigh-wave time traces used for the inversions at stations PPDB and AGVB. Figure 8 shows the final waveform (time domain) fitting results of the inversions. The solid traces are the observed waveforms, and the dashed traces the synthetic waveforms. The amplitude for R0 at PPDB in particular appears to decrease rapidly for periods longer than about 25 s, yet the group-velocity plot (Figure 6) suggests that surface-wave energy extends to periods well in excess of 100 s. Efforts to enhance the long-period end of the PPDB R0 record by low-pass filtering and including that long-period time series as an additional trace in the inversion did not significantly affect the solution. These additional long-period R0 traces were not included in the final inversions.

The model is poorly constrained at depths below about 150 km for these data, so some method of damping is required to produce stable solutions. We used Ridge Regression (which is equivalent to Variance-

Table 4. Group-Velocity and Frequency-Band Limits for the Time Traces Used in the Waveform Inversion

Mode	Station	GV Low	GV High	FB Low	FB High
R0	AGVB	2.45	3.59	0.009	0.06
R0	PPDB	2.58	3.55	0.006	0.07
R1	AGVB	3.43	4.41	0.05	0.085
R1	PPDB	2.67	4.40	0.05	0.098

GV, group velocity; FB, frequency band.

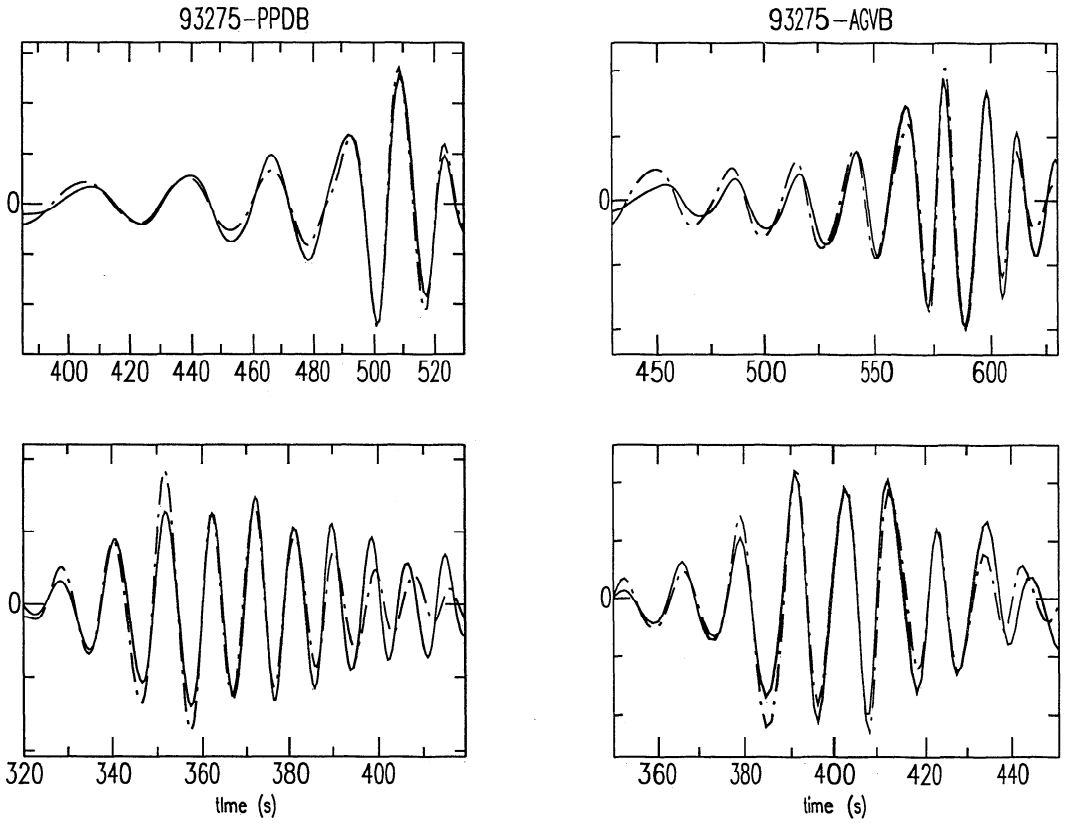

Figure 8. Time series for the predicted and observed ground-displacement traces at (left) PPDB and (right) AGVB from event 93275. The top panels show R0 and the bottom panels show R1. The solid lines are the data and the dash-dotted lines are the synthetics. The data and synthetics have identical bandpass filtering in each case, and they have been equalized in energy.

Spread Trade-Off) [*Menke*, 1989] with a damping of 0.01 km/s. This level of damping results in a covariance increase by about a factor of 5 from the Moho to 300 km depth with resolution of the order of the model parameters (Figure 7).

The output velocity-depth models from the waveform inversion are for a mixed path and therefore have no direct relationship to the Earth. The calculated R0 phase-velocity curve for the mixed path is shown in Figure 9. These, along with the other dispersion curves derived from the mixed-path final model, are used below for the pure-path solution for the Chaco Basin.

To isolate the Chaco Basin structure requires an estimate of the structure for the western Paraná Basin. We need first to determine if the velocity-depth structure of the western Basin is similar to that of the eastern Paraná Basin, for which we have a much larger data set. The limited data for the western Paraná is due to the very short period of deployment of station PTMB on the western boundary of the basin. Thus, only a single event, 94344 (Table 1), traverses an interstation great-circle path (PTMB–AGVB) that is confined to the western Paraná Basin. Both Love and Rayleigh waves were well recorded at PTMB, but the data are limited for longer periods at AGVB. The data provide estimates of fundamental-mode Love and Rayleigh interstation phase velocities in the period range 20–65 s for Rayleigh and 10–43 s for Love. Within error, data-derived dispersion curves shown in Figure 9 agree with the dispersion curves labeled E_PARANA, predicted from the model for the eastern Paraná Basin (Figure 5), consistent with a relatively homogeneous structure across the whole of the Paraná Basin. Using this assumption, we can partition the 93275-AGVB and 93275-PPDB paths into Paraná Basin and Chaco Basin segments and solve for the velocity structure beneath the Chaco Basin.

As shown in Figure 9, we then have data-derived estimates for the Paraná phase velocity c_P and the mixed-path Chaco-Paraná phase velocity c_{CP}. We estimate from surface geology that the propagation path for event 93275 to stations AGVB or PPDB is about 55% Chaco Basin and about 45% Paraná Basin. We can therefore calculate the Chaco phase velocity c_C for discrete frequencies from the expression

$$\frac{0.55}{c_C} = \frac{1}{c_{CP}} - \frac{0.45}{c_P}.$$

Results for Rayleigh and Love fundamental-mode phase velocities are shown in Figure 9.

The same procedure can be used to derive first higher-mode Rayleigh phase and fundamental-mode Love and Rayleigh group velocities as well, where we restrict the period ranges to those used for the eastern Paraná analysis described above (Figure 5; Table 3).

The Chaco pure-path dispersion values so derived were then inverted to obtain an S-wave velocity-depth

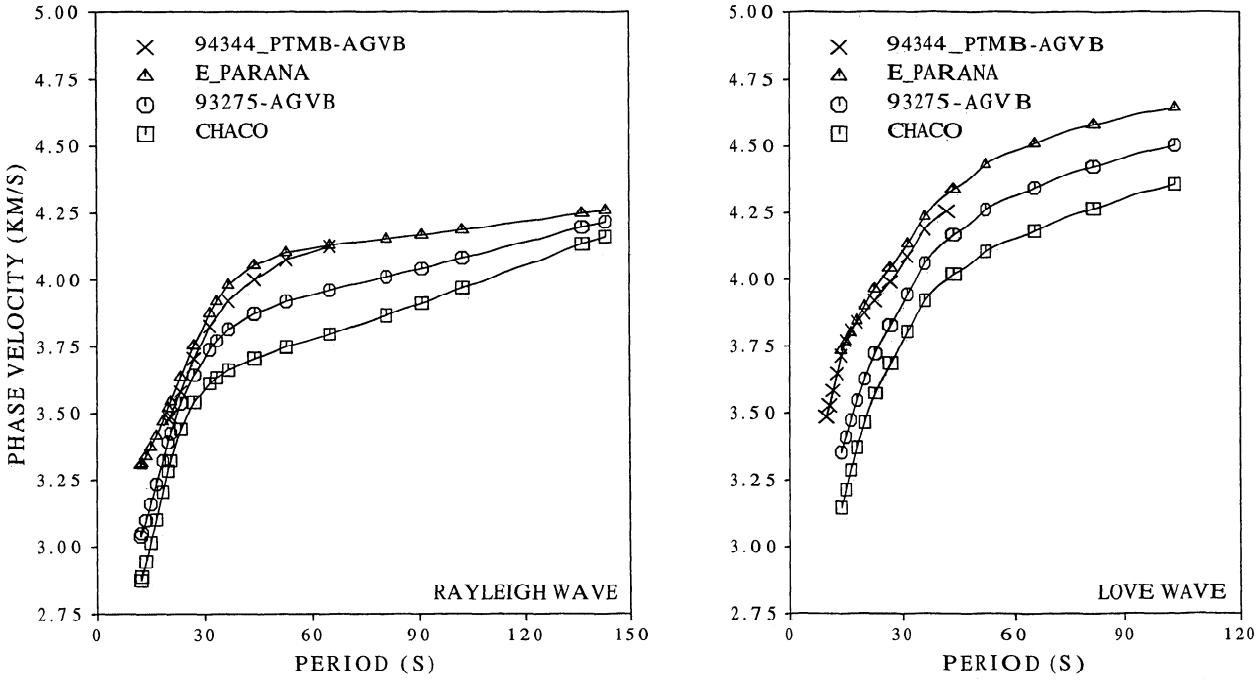

Figure 9. Fundamental-mode Rayleigh and Love phase-velocity dispersion curves. The 94344_PTMB-AGVB curves are derived directly from the dispersion data; the E_PARANA curves are derived from the PARANA model (Figure 5); the 93275-AGVB curves are derived from waveform inversion (Figure 8); and the CHACO curves are derived from E_PARANA and dispersion curves derived from the 93275-AGVB and 93275-PPDB models (see text).

model for the Chaco Basin. The dispersion input included Chaco values estimated using both the 93275-AGVB model and the 93275-PPDB model. The velocity model for 93275-AGVB with a modified crust was taken as a starting model for the inversion: the crustal model had a low-velocity sedimentary layer in the upper 3.5 km and a Moho at 32 km. *P*-wave velocities and densities remained fixed during the inversion.

The velocity-depth model for the Chaco Basin is shown in Figure 10, along with the Paraná model and the IASPEI91 model as reference. We do not present a formal error estimate for the velocity structure, but because it is based on only a single (albeit well recorded) event, the model cannot be considered to be as well constrained as the Paraná Basin model. We feel, however, that it is reasonable to conclude that the differences between the Chaco and Paraná models in the uppermost mantle are significant to at least 150 km depth.

Discussion and Conclusions

The velocity structure beneath the Paraná Basin is characteristically shield-like. The uppermost mantle consists of a high velocity (4.7 km/s) "lid" that overlies mantle material of gradually decreasing velocity, with velocities reaching about 4.6 km/s at 200 km depth. These mantle velocities, which appear to be quite consistent across the whole of the Paraná Basin, are still well above asthenospheric values: there is no evidence for an upper mantle low-velocity zone anywhere beneath the Paraná Basin. From this we judge that the Paraná plume, while it presumably affected the lower continental lithosphere, did not result in formation of a lasting asthenospheric zone beneath the Paraná Basin. The generation of Paraná flood basalts may even have contributed to the formation of the observed high velocity "lid" beneath the Basin, a result of olivine-rich cumulate crystallization in the upper mantle. We find nothing in the Paraná Basin velocity-depth structure to shed light on the question of why the region was one of continuous subsidence over hundreds of millions of years during Paleozoic and Mesozoic time.

The striking contrast in velocity structure between the Chaco Basin and the Paraná Basin is an unexpected result of this study. The crust of the Chaco Basin is only about 32 km thick, substantially thinner than that beneath the Paraná Basin, and the modeled crustal velocities may be slightly lower, although crustal velocities are poorly constrained by the model. The uppermost mantle velocities beneath the Chaco, however, are calculated to be about 4.2 km/s, characteristic of asthenospheric mantle. Unlike the Paraná Basin, the mantle velocities beneath the Chaco are lowest at the base of the crust and gradually increase with depth to about 4.4 km/s at 200 km depth, still lower than those of the Paraná Basin.

While the significance of the apparent low upper mantle velocities beneath the Chaco Basin is wholly speculative at this point, at least two possibilities present themselves. First, the low velocities could be related to the Andean arc. In particular, the low-lying Chaco Basin is situated in the region of the arc where back-arc

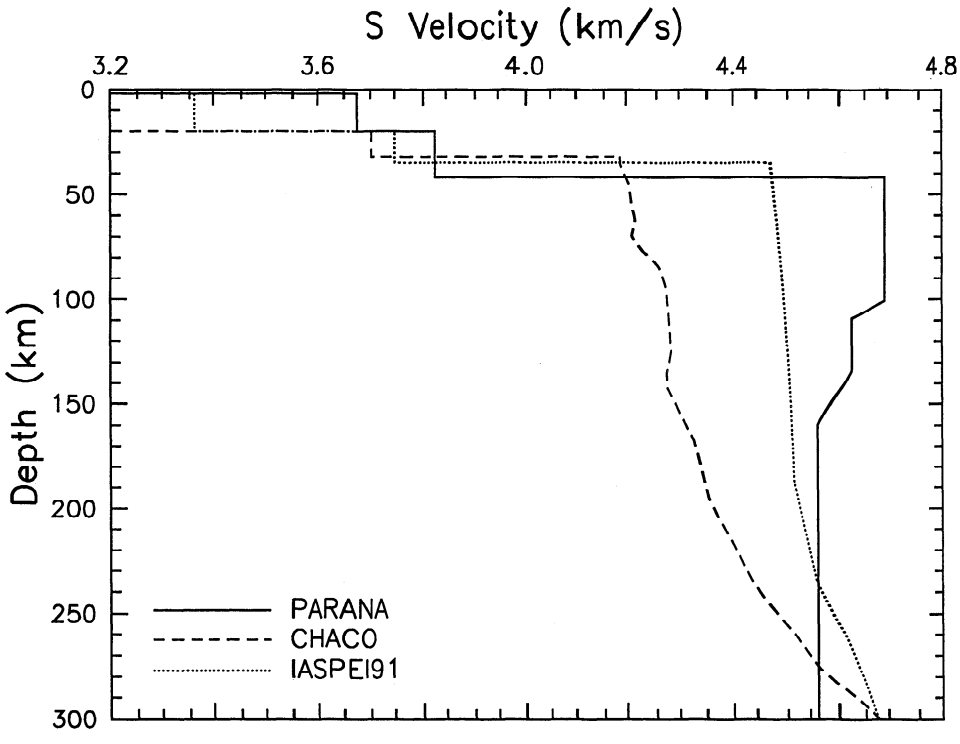

Figure 10. Velocity-depth models for the Chaco and Paraná Basins derived in this study. Also included is the IASPEI91 model as a reference. The displayed model layer transitions have been smoothed except for intended first-order discontinuities.

spreading does occur beneath oceanic island arcs, and the velocity structure, both crustal and upper mantle, could be indicative of hotter mantle and perhaps crustal stretching. On the other hand, the only tectonism associated with the Andean back arc, including subandean crustal earthquakes, appears to be compressional, not extensional, and we would therefore not expect extension beneath the Chaco Basin. Heat flow measurements, which might be definitive in this case, are lacking in the Basin proper, although measurements on the border between the sub-Andean zone and the Chaco Basin in Bolivia appear to be in the range of normal shield values [*Henry and Pollack*, 1988].

Low upper-mantle velocities need not necessarily imply high temperatures. *Ramos'* [1988] reconstruction of the Chaco region of South America shows late Proterozoic subduction zones that bounded the region at different times on both its eastern and its western flanks, with the descending plate in both cases dipping beneath the Chaco region. In addition, the axis of an inferred Paleozoic back-arc spreading center is situated close to the axis of the Chaco Basin [*Ramos*, 1988]. If this reconstruction is correct, then subduction activity could possibly have left behind a hydrated, metasomatized mantle with seismic velocities reduced relative to those of "normal" mantle. We note in this regard, however, that the observed mantle velocities, if they are confirmed by further measurement, appear to be lower than would be expected even for severely hydrated and metasomatized old continental mantle. Moreover, part of the surface-wave path across the Chaco Basin traverses an area presumed to be underlain by a northern arm of the Rio de la Plata craton [*Ramos*, 1988], an Archean crustal block which at least at one time should have been characterized by a high-velocity mantle root.

Acknowledgments. Special acknowledgment is due our principal collaborator in Brazil, Marcelo Assumpção of the University of São Paulo, whose insight and leadership played a major role in the success of the BLSP experiment. In addition, we thank him for comprehensive criticism of an earlier draft that resulted in a significantly improved manuscript. We acknowledge major contributions of our close collaborators in Brazil who participated in the BLSP experiment, including IPT (Luis Carlos Ribotta), CESP (high-level technical support), UNESP in Presidente Prudente (technical support), CEMIG and FURNAS, in addition to the University of São Paulo. The installation, operation, and maintenance of the broadband instruments would not have been possible without the indispensible services and talents of Carnegie Institution's Randy Kuehnel: we acknowledge his contribution to this work and to the Carnegie broadband program. Particular appreciation is due Guust Nolet for providing the partitioned waveform inversion programs, for many helpful conversations about their use and interpretation, and for thorough review of the manuscript. We owe special thanks to Suzan Van der Lee for many stimulating discussions on various aspects of partitioned waveform inversion and for help in confirming some of the results. Bob Herrmann kindly provided current versions of his surface-wave inversion programs and offered suggestions for their use. Map plots were done using GMT [*Wessel and Smith*, 1991] and seismic plots using Seismic Analysis Code (SAC), the latter provided by Lawrence Livermore National Laboratory of the University of California. This work is supported by grants from the NSF-US (EAR-9304503), FAPESP-Brazil, and PADCT-Brazil.

References

Aceñolaza, F. G., El sistema Ordovícico en Sudamérica, *Acta Geol. Lilloana, 16*, 77–91, 1982.

Bloch, S., A. Hales, and M. Landisman, Velocities in the crust and upper mantle of Africa from multi-mode surface wave dispersion, *Bull. Seismol. Soc. Am., 59*, 1599–1629, 1969.

Brito Neves, B., and U. Cordani, Tectonic evolution of South America during the late Proterozoic, *Precambrian Res., 53*, 23–40, 1991.

Brito Neves, B. B., R. Fuck, U. G. Cordani, and A. Thomaz, Influence of basement structures on the evolution of the major sedimentary basins of Brazil: A case of tectonic heritage, *J. Geodyn., 1*, 495–510, 1984.

Cordani, U. G., B. B. Brito Neves, R. A. Fuck, R. Porto, A. T. Filho, and F. M. Bezerra da Cunha, Estudo preliminar de integração do Pré-cambriano com os eventos tectônicos das bacias sedimentares brasileiras, in *Revista Cienca Tecnica Petroleo, Rep. 15*, 70 pp., Petrobrás, Centro de Pesquisas e Desenvolvimento Leopoldo A. Maguez de Mello (CENPES), Rio de Janeiro, Brazil, 1984.

Coudert, L., M. Frappa, C. Viguier, and R. Arias, Tectonic subsidence and crustal flexure in the Neogene Chaco basin of Bolivia, *Tectonophysics, 243*, 277–292, 1995.

Dziewonski, A., S. Bloch, and M. Landisman, A technique for the analysis of transient seismic signals, *Bull. Seismol. Soc. Am., 59*, 427–444, 1969.

Gallagher, K., and C. J. Hawkesworth, Dehydration melting and the generation of continental flood basalts, *Nature, 358*, 57–59, 1992.

Henry, S. G., and H. N. Pollack, Terrestrial heat flow above the Andean subduction zone in Bolivia and Peru, *J. Geophys. Res., 93*, 15153–15162, 1988.

Herrmann, R. B., *Computer Programs in Seismology*, St. Louis University, St. Louis, Mo., 1987.

Hwang, H. J., and B. J. Mitchell, Shear velocities, Q_β, and the frequency dependence of Q_β in stable and tectonically active regions from surface wave observations, *Geophys. J. R. Astron. Soc., 90*, 575–613, 1987.

James, D. E., JB or not JB?: Yet another look at *P*-wave velocities in the upper-mantle transition zone, (abstract) *Eos Trans. AGU*, 75-(16), Spring Meet. Suppl., 233, 1994a.

James, D. E., *P* and *S* seismic velocities in the upper-mantle transition zone beneath the western Brazilian shield, *Extended Abstracts of the International Symposium on the Physics and Chemistry of the Upper Mantle*, Brazilian Academy of Sciences and University of São Paulo, São Paulo, Brazil, 124–126, 1994b.

James, D. E., and M. Assumpção, Tectonic implications of *S*-wave anisotropy beneath SE Brazil, *Geophys. J. Int., 126*, 1–10, 1996.

James, D.E., M. Assumpção, J. A. Snoke, L. C. Ribotta, and R. Kuehnel, Seismic studies of continental lithosphere beneath SE Brazil, *Ann. Acad. Bras. Cien., 65*, suppl. 2, 227–250, 1993.

Lesquer, A., F. F. M. Almeida, A. Davino, J. C. Lachaud, and P. Maillard, Signification stucturale des anomalies gravimetriques de la partie sud du craton de Sao Francisco (Brésil), *Tectonophysics, 76*, 273–293, 1981.

Menke, W., *Geophysical Data Analysis: Discrete Inverse Theory*, Academic, San Diego, Calif., 1989.

Mitchell, B. J., On the inversion of Love- and Rayleigh-wave dispersion and implications for Earth structure and anisotropy, *Geophys. J. R. Astron. Soc., 76*, 233–241, 1984.

Nolet, G., Linearized inversion of (teleseismic) data, in *The Solution of the Inverse Problem in Geophysical Interpretation*, edited by R. Cassinis, pp. 9–37, Plenum, New York, 1981.

Nolet, G., Partitioned waveform inversion and two-dimensional structure under the network of autonomously recording seismographs, *J. Geophys. Res., 95*, 8499–8512, 1990.

Nyman, D. C., and M. Landisman, The display-equalized filter for frequency-time analysis, *Bull. Seismol. Soc. Am., 67*, 393–404, 1977.

Ramos, V. A., Late Proterozoic-Early Paleozoic of South America — A collisional history, *Episodes, 11*, 168–174, 1988.

Russell, D. R., Multi-channel processing of dispersed surface waves, *Ph.D. thesis*, St. Louis Univ., St. Louis, Mo., 1987.

Sempere, T., G. Hérail, J. Oller, and M.G. Bonhomme, Late Oligocene-early Miocene major tectonic crisis and related basins in Bolivia, *Geology, 18*, 946–949, 1990.

Taylor, S. R., and M. N. Toksoz, Measurement of interstation phase and group velocities and Q using Wiener filtering, *Bull. Seismol. Soc. Am., 72*, 73–91, 1982.

VanDecar, J. C., D. E. James, and M. Assumpção, Seismic evidence for a fossil mantle plume beneath South America and implications for plate driving forces, *Nature, 378*, 25–31, 1995.

Wessel, P., and W. H. F. Smith, Free software helps map and display data, *Eos Trans. AGU, 72*-(41), 445–446, 1991.

D. E. James, Department of Terrestrial Magnetism, Carnegie Institution of Washington, 5241 Broad Branch Road, N.W., Washington, D.C., 20015. (e-mail: james@dtm.ciw.edu)

J. A. Snoke, Virginia Tech Seismological Observatory, Department of Geological Sciences, Virginia Tech, Blacksburg, VA 24061-0420. (e-mail: snoke@vt.edu)

(Received April 25, 1996; revised September 30, 1996; accepted October 14, 1996.)